Photocatalytic activity and electron storage capability of TiO_2 aerogels with adjustable surface area

Alexandra Rose[a,§], Anja Hofmann[b,§], Pascal Voepel[a], Barbara Milow[a], Roland Marschall[b,]*

Abstract. Mesoporous TiO_2 aerogels with surface area larger than 600 m^2 g^{-1} have been prepared *via* acid-catalyzed sol-gel synthesis and supercritical drying. Varying temperature treatment in air results in changes in the morphology of the aerogels and their specific surface area. Interestingly, the ability to store photogenerated electrons in the surface states of the aerogels upon illumination of dispersions in water-methanol mixtures increases with lower calcination temperature. Additionally, the extent of electron storage capability also depends on hole scavenger concentration. Increasing the calcination temperature to 500 °C results in decreased surface area and electron storage capability, however in increased hydrogen evolution rates. Finally, nitrogen reduction to ammonia in the dark is performed with photogenerated stored electrons in TiO_2 aerogels, separating the charge carrier photogeneration from the dark reduction reaction.

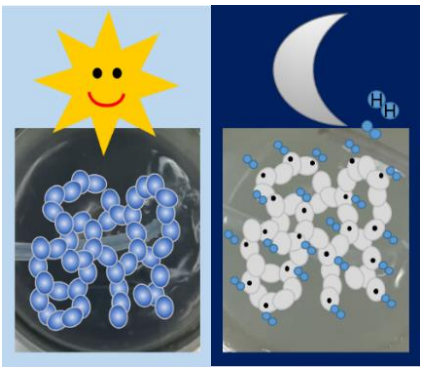

Keywords: TiO_2 aerogel, Electron storage, Photocatalysis, Hydrogen production, Nitrogen reduction

1. Introduction

Aerogels are unique 3D mesoporous materials of interconnected porous networks which exhibit high surface areas, open pores and low densities.[1,2] The sol-gel process is a prominent technique to synthesize such aerogels, since it is a simple method and requires no complex setup. Several synthesis parameters can be varied to control the nanoscale structure and physicochemical properties.[3,4] It has been demonstrated that high surface areas could be obtained in amorphous titania aerogels based on chloride and alkoxide precursors followed by hydrolysis and condensation reaction forming a wet gel[5,6] which is further dried e.g. supercritically to prevent the porous structure to collapse.[1] The ability to control the sol-gel process for synthesizing aerogels is a powerful tool for designing a suitable and efficient catalyst. A high specific surface area and open porosity of aerogels favors the adsorption and diffusion of reactants, therefore offers many active reaction sites and their accessibility for photocatalytic reactions.[7] The interconnected network of nanoparticles offers additionally long diffusion pathways for photogenerated electrons.

Aerogels were reported as suitable catalysts for photocatalytic applications, e.g. degradation of dyes or organic substances and hydrogen evolution.[8–12]. Especially, TiO_2 and composite aerogels are high potential materials for efficient photocatalysis, due to reactive sites and improved charge separation.[13,14] The polymorphic forms of TiO_2, and morphological and

[a] A. Rose, Dr. P. Voepel (ORCID:0000-0001-8233-7261), Prof. Dr. B. Milow (ORCID: 0000-0002-6350-7728)
German Aerospace Center
Institute of Materials Research
Aerogels and Aerogel composites
Linder Höhe, Köln 51147, Germany

[b] A. Hofmann, Prof. R. Marschall
Department of Chemistry
University of Bayreuth
Universitätsstraße 30, Bayreuth 95447, Germany
*E-mail: roland.marschall@uni-bayreuth.de , ORCID: 0000-0002-1057-0459

§: These authors contributed equally to the manuscript.

structural characteristics were reported as crucial factors for photocatalysis. Different synthesis procedures for TiO_2 aerogels are reported in literature, to improve synthesis parameters and consequently the morphological and structural characteristics with regard to photocatalytic hydrogen evolution.

Parayil *et al.* investigated the synthesis parameters using alkoxide precursors for TiO_2 aerogel synthesis *via* high temperature supercritrical drying.[15] Luna *et al.* reported TiO_2 aerogels assembled from crystalline pre-formed nanoparticles which showed an efficient hydrogen generation.[8] Recently, Niederberger *et. al.* presented similar titania-based aerogels and their ability for hydrogen production based on water/methanol vapours.[16] TiO_2-Pt composites were reported by Lin *et al.* and Puskelova *et al.*[17,18] They described the dependency of the hydrogen evolution rate on the Pt particle size and loading on TiO_2, reflecting the number of reactive sites. With intensity-modulated photovoltage spectroscopy and photocurrent spectroscopy measurements on TiO_2 aerogels, synthesized with different weight fractions of sol-gel precursors, DeSario *et al.* were able to show that trapping sites are the reactive sites in photocatalytic hydrogen generation.[13] This could be concluded due to differences in lifetime and mobility of photogenerated electrons. Hydrogen generation increased with increased sol-gel precursor concentration. By use of UV-Vis and EPR spectroscopy, Di Iorio *et al.* found an improved electron storage capacity for TiO_2 ethanolic sols with an increase of titanium to water molar ratio.[19] Panayotov *et al.* reported that photogenerated electron-hole pairs in TiO_2 aerogels are more efficiently separated compared to commercial TiO_2 nanoparticles and that the density of excited-state electrons is higher in these aerogels.[14]

Besides the discussed aerogel structure, the crystal structure also has an influence on the charge carrier lifetime. Sachs *et al.* performed transient absorption spectroscopy measurements on the most commonly used TiO_2 crystals phases, i.e. rutile and anatase. They found a faster recombination rate for the rutile crystal phase and that for both polymorphs, the surface recombination is the most important factor for the charge carrier lifetime.[20]

There are several examples in the literature which report the storage of photoexcited electrons in semiconductor materials, and the use of these stored electrons for reduction reactions. Bahnemann *et al.* reported the trapping of electrons close to the surface of colloidal TiO_2 with the formation of Ti^{3+} states in presence of a hole scavenger, which was characterized by a broad absorption with a maximum at 650 nm.[21] They performed further investigation on the electron storage of TiO_2. By employing the stopped flow technique and UV-Vis spectroscopy, they investigated the reduction reaction of the stored electrons with silver ions[22], gold ions[23], and other electron acceptors in detail.[24,25] In 2011, they showed for the first time that photoexcited electrons stored in TiO_2 can reduce nitrogen.[26] Since then, reports about the electron storage of different materials[27] including WO_3,[28] copper complexes,[29] and carbon nitrides[30] were published. In case of cyanamide-functionalized polymeric networks of heptazine units, 4-methylbenzyl alcohol was necessary as hole acceptor to store electrons in the material. In contrast to this, an aqueous methanol solution with a concentration of 0.02 mol L^{-1} is already enough to extract photoexcited holes and to store photoexcited electrons in TiO_2.[26] The addition of a co-catalyst like Pt or other metal co-catalysts to a photocatalyst storing photoexcited electrons in aqueous solution, lead to the formation of hydrogen.[22,23,30,31]

In the present work, we report a detailed investigation on the photocatalytic and electron storage properties of mesoporous TiO_2 aerogels prepared *via* a novel modified acid catalyzed sol-gel synthesis with subsequent supercritical drying and different heat treatments in air. All prepared TiO_2 aerogels exhibit the anatase crystal structure to exclude the influence of a composite formation on the photocatalytic activity and electron storage ability of the aerogels. The influence of the physical properties, especially the surface area and crystallinity, on the ability to store electrons in water-methanol slurry and on hydrogen evolution are discussed in detail. Methanol concentration-dependent measurements on samples with high electron storage ability are presented furthermore, and *via* an experiment for nitrogen reduction in the dark yielding ammonia, using such stored electrons as a possible ammonia-on-demand application for the herein synthesized aerogels a highly promising application besides hydrogen generation is presented.

2. Experimental Section

2.1 Chemicals

Titanium (IV) tetraisopropoxide (98%, Merck), hydrochloric acid (37%, ACS reagent, Sigma Aldrich), ethanol (Chemcolute, denatured with MEK, IPA, and Bitrex, 99.8%), methanol (99.9%, Fisher chemical), hexachloroplatinate (IV) hydrate (99.995%, Carl Roth) were used as received.

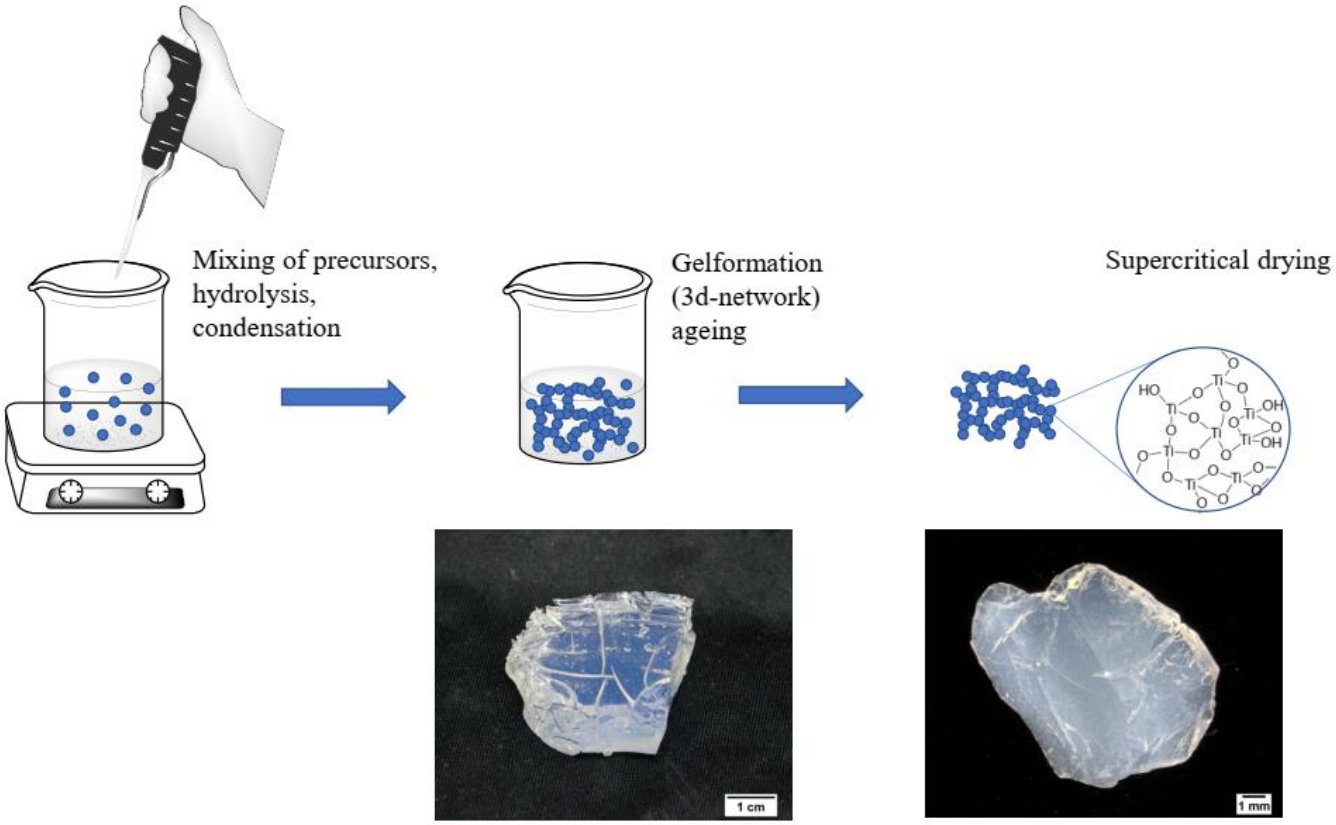

Scheme 1. Schematic presentation of synthesis procedure and images of TiO_2 wet gel (left) and aerogel (right).

2.2 TiO_2 aerogel synthesis (Scheme 1)

TiO_2 gels were prepared with acid (HCl) catalyzed sol-gel method using titanium (IV) isopropoxide (TTIP) as precursor. The molar ratio of TTIP/ethanol/acid/water was kept constant 1 : 26 : 0.1 : 4. A solution containing TTIP in ethanol (EtOH) was prepared under magnetic stirring at 0 °C. Hydrochloric acid was added after few minutes. Deionized water was added dropwise to the solution. A gel formed after few minutes. Gels were aged for 7 days at 50 °C, then washed in isopropanol four times and dried with CO_2 at supercritical conditions (60 °C, 115 bar, flow rate 15-20 kg/h). As formed aerogels, excluding as-synthesized aerogel, were thermally treated in air at 300 °C, 400 °C, and 500 °C for 10 h (heating rate 10 K min^{-1}).

2.3 Characterization

XRD measurements were performed on a Bruker D8 Advance X-ray diffractometer using Cu-K_α radiation source and Lynxeye XE-T detector. The diffraction data were collected in the range of 15-90° 2θ with a step size of 0.01°. The crystallite sizes were estimated using Bruker EVA software by calculating the integral breadth from XRD pattern. Phase quantification and determination of amorphous/crystalline phase was performed by the Rietveld method implemented in Topas using CeO_2 as internal standard.

The specific surface area was determined via N_2 physisorption measurements at 77 K on a Micromeritics 3Flex instrument in a partial pressure range of $0.05 < p/p^0 < 0.3$ using the Brunauer-Emmett-Teller (BET) method. The total pore volume of the samples was obtained from the N_2 desorption isotherms at a partial pressure of 0.98, and the pore size distribution was obtained using Barrett-Joyner-Halenda (BJH) model. Prior to physisorption analysis, the samples were outgassed at 60 °C for 12 h on a Micromeritics VacPrep Gas Adsorption Sample Preparation Device.

SEM images were taken with a Zeiss Ultra 55 electron microscope using an accelerating voltage of 3 kV. The samples were coated with platinum using a Baltec sputter coater prior to measuring.

TEM analysis was performed with a Philips Tecnai F30 operated at 300 kV. D-spacing was determined from TEM images using ImageJ.

A PerkinElmer Lambda 750 UV/vis/NIR spectrometer, equipped with a Praying-Mantis mirror unit from Harrick, was used to record the diffuse reflectance of the powdered aerogels with a step size of 1 nm. The used white standard was a spectralon pellet. The spectra were converted into absorption spectra using Kubelka-Munk function. Tauc plots were used to estimate the band gaps. For the estimation of the absorbance of the dispersions, the spectrometer was equipped with an integrating sphere, and the dispersion was stirred during the measurements of the diffuse reflectance. The spectra

were converted to absorbance spectra. Three measurements were performed for every point and error was determined.

2.4 Photocatalytic test experiments

For all photocatalytic experiments ultrapure water with TOC = 2 ppb was used. The experiments were conducted with a 300 W Xe lamp (Quantum Design) in a top-irradiated glass reaction vessel. Measurements were all performed at 20 °C (ECO RE 1050G (Lauda) thermostat) under stirring. The system was flushed with argon 5.0 before the measurements to remove residual air. Detection of the evolved hydrogen was performed every 11 minutes using a GC2014 gas chromatograph from Shimadzu, equipped with a shin carbon ST column (Restek) and a thermal conductivity detector, using argon 5.0 as carrier gas. The argon 5.0 flow rate for the measurements was set to 25 mL min^{-1} with a Bronkhorst mass flow controller.

The hydrogen evolution experiments with Pt photodeposition were carried out with 100 mg aerogel sample dispersed in a mixture of 135 mL water and 15 mL methanol. The dispersion was irradiated for 100 min without co-catalyst. The lamp was turned off and it was waited until no hydrogen evolution was detected anymore, then an aqueous solution of hexachloroplatinate (IV) hydrate was added via rubber sealing without opening the reactor to reach 0.0076 µmol m^{-2}. The lamp was turned on again after the hydrogen evolution peak, and the sample was irradiated for another 100 min. Afterwards the lamp was turned off, and it was waited that the hydrogen evolution was zero. Another amount of hexachloroplatinate (IV) hydrate was added to the calcined aerogel dispersion to reach the same amount of 0.1 wt.-% Pt as for the as-synthesized aerogel sample. The dispersions of the calcined aerogel samples were irradiated again for 100 min, the lamp was turned off and the measurements were stopped after no hydrogen evolution was detected. Photographs of all dispersions were taken before the measurement and after each irradiation step. The samples with Pt deposited were washed with isopropanol three times and centrifuged at 1500 rpm. Then they were dried with CO_2 at supercritical conditions. XRD measurements were performed as described above to determine any changes on the sample.

For the experiments to detect the absorbance of the dispersions, 100 mg of the aerogel sample were dispersed in a mixture of 135 mL of water and 15 mL methanol. After flushing with argon 5.0, a sample of approximately 2.5 mL dispersion was taken and filled in an argon flushed closed cuvette, and the diffuse reflectance was measured in a PerkinElmer Lambda 750 UV/vis/NIR spectrometer, equipped with an integrating sphere under stirring. The aerogel dispersions were afterwards irradiated for 100 min. 2.5 mL of the blueish dispersion was filled in an argon flushed cuvette and the diffuse reflectance was measured immediately, 30 minutes, and 110 min after the sample was taken.

For the experiments of the dependency of the electron storage ability on the methanol concentration, 100 mg of the as-synthesized aerogel sample were dispersed in 150 mL aqueous methanol solutions with different methanol concentrations ranging from 0.02 mol L^{-1} up to 19.7 mol L^{-1}. The dispersions were irradiated for 100 min. Photographs of the dispersions were taken directly after the irradiation.

For the nitrogen reduction reaction, 100 mg of the as-synthesized aerogel was dispersed in 150 mL of 2.5 mol L^{-1} aqueous methanol solution. The dispersion was irradiated for 100 min under the same conditions as for the absorbance detection measurements, the argon 5.0 flow rate was set to 50 mL min^{-1}. After the irradiation under argon 5.0, the carrier gas was switched to N_2. The flow rate was set to 50 mL min^{-1} N_2 for 7 h for the nitrogen reduction reaction in the dark. Afterwards a salicylate test was performed to determine the yield of NH_3.[32]

3 Results and Discussion

3.1 Sample Characterization

The synthesized TiO_2 gel (Scheme 1 left photograph) shows a transparent appearance. After supercritical drying the as-synthesized TiO_2 aerogel (Scheme 1 right photograph) turned into a very light, brittle and translucent aerogel. The translucency in the visible range indicates a small particle size and homogeneous pore distribution,[33] which is confirmed by the physisorption results shown in **Figure 2**.

X-ray diffraction (XRD) patterns of the as-synthesized and calcined TiO_2 aerogels are shown in **Figure 1.** It can be observed that surprisingly the as-synthesized TiO_2 aerogel (please see *Experimental Section* for details) is semi-crystalline. The broad diffraction peaks represent a high amorphous content, but the main reflections at 25.28° and 48.05° 2θ agree with the main reflections of anatase TiO_2 (PDF-21-1272). TiO_2 nanostructures which are synthesized using TTIP were reported to be crystalline (anatase) when ambiently dried or dried at e.g. 60°C.[34,35] However, in our case, the TiO_2 gels were, supercritically dried, which generally as reported in literature lead to amorphous aerogels. Varying the synthesis conditions e.g type or amount of catalyst, without any addition/assembly of preformed crystalline

TiO_2 nanoparticles, the resulting aerogels were reported to be amorphous or only very few crystallites were found.[5,6,8,16,36]

The degree of crystallinity was determined with Rietveld refinement using an internal standard, that indicated a significant crystalline content of TiO_2 anatase in the as-synthesized aerogel (**Table 1**). The degree of crystallinity of the as-synthesized TiO_2 aerogel could be due to the temperature and pressure during the supercritical drying process. It was reported by Moussaoui *et al.* that the drying conditions, such as high temperature, have an impact on the crystalline structure.[37]

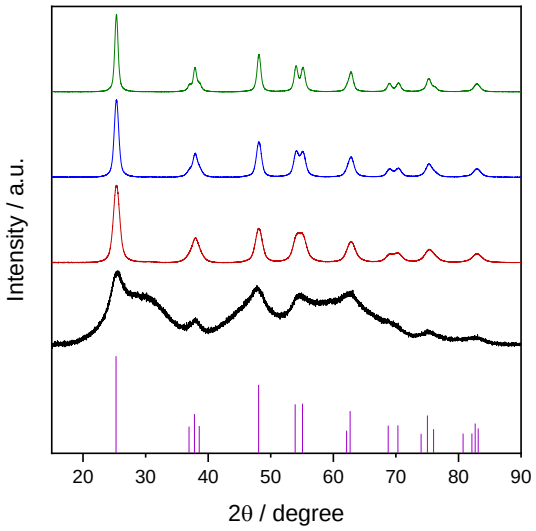

Figure 1. XRD patterns of the as-synthesized TiO_2 aerogel (black) and aerogels calcined at 300 °C (red), 400 °C (blue) and 500 °C (green). Reference line pattern of anatase TiO_2 (PDF-21-1272) is shown for comparison. Normalized data to the range 0 to 100 related to the highest signal.

The heat-treated TiO_2 aerogels at 300°C, 400°C and 500°C show reflections which can be assigned to the TiO_2 anatase crystal structure. No reflections can be assigned to TiO_2 rutile crystal structure, which is ideal for photocatalytic applications, since rutile is usually less active.[38] According to literature, anatase is the most likely occurring crystal structure at the applied calcination temperatures.[6] The anatase-rutile phase transition was reported to occur at temperatures between 400-800 °C.[3] The XRD pattern of the calcined aerogel at 500 °C exhibits well-defined and better resolved reflections compared to the calcined aerogels at 300 °C and 400 °C, respectively. This indicates that the crystallinity increases with the calcination temperature. The crystallite sizes of the aerogels were estimated for (101) preferred oriented anatase TiO_2 in the range of 23°-28° *2θ*. They increase with calcination temperature from 4 nm for the as-synthesized TiO_2 aerogel to 13 nm for TiO_2 aerogel calcined at 500 °C (**Table 1**).

In order to study the influence of the calcination temperature on the degree of crystallinity of TiO_2 aerogels, Rietveld refinement was applied on the XRD data of the prepared samples (**Table 1**). The semi-crystalline structure of the as-synthesized TiO_2 aerogel was confirmed with a maximum crystalline content of approx. 10 wt.%. For calcination temperatures of 300°C-500°C the TiO_2 sample was completely crystallized forming anatase.

Table 1. Rietveld analysis of the prepared TiO_2 aerogel samples

	TiO_2 crystalline phase/anatase wt.%	TiO_2 amorphous phase wt.%	Crystallite size / nm
as-synthesized	10	90	4
300 °C	100	0	7
400 °C	100	0	10
500 °C	100	0	13

The adsorption and desorption isotherms of the as-synthesized and heat-treated TiO_2 aerogels are presented in **Figure 2**. They exhibit a type IVa isotherm with H1 hysteresis loop according to the IUPAC classifications indicating a mesoporous material.[39] The desorption path is in thermodynamic equilibrium and different to the adsorption path, leading to hysteresis which is associated with delayed capillary condensation during adsorption.[40,41] The type H1 hysteresis loop and the steep adsorption branch indicate a uniform and narrow pore size distribution. The adsorbed volume of nitrogen increases strongly at a relative pressure of p/p^0=0.6 for the as-synthesized TiO_2 aerogel before it reaches a plateau, indicating capillary condensation and saturation. For the heat-treated TiO_2 aerogels the steep adsorption branch occurs at higher relative pressures, in particular the higher the calcination temperature the higher the relative pressure for the increase of adsorbed volume. This indicates larger pores after higher calcination temperatures. This is in good agreement with the pore size distribution shown in **Figure 2 (inset)**.

A narrow pore size distribution was obtained for the as-synthesized and heat-treated TiO_2 aerogels, whereby the pore size distribution is slightly narrower and the BJH-derived average pore size shifts to larger pore sizes for the heat-treated samples. This is in good agreement with the location of hysteresis loops, which occur at higher relative pressure and in a narrower pressure range for higher calcination temperatures. This can be explained by smaller mesopores (approx. 5-15 nm) which coalesced with larger mesopores (approx. 20 nm). The reduced number of smaller mesopores could also explain the decreased surface area after heat-treatment, as smaller pores contribute more to higher surface areas.[6]

The physisorption results are summarized in **Table 2**. It shows the effect of calcination temperature on the specific surface area and cumulative pore volume. The as-synthesized TiO_2 aerogel exhibits high specific surface area and pore volume of 600 m^2/g and 2.5 cm^3/g, respectively. The supercritical drying process preserves the mesoporous structure of the as-synthesized TiO_2 aerogel leading to the observed high values. Similar results have been reported in literature by Sadrieyeh *et al.*, however the aging time could be reduced from >40 days to 7 days during synthesis here, achieving a stable and translucent TiO_2 aerogel.[6] As expected, the surface area as well as the pore volume decrease for the heat-treated TiO_2 aerogel at 300 °C. The surface area and pore volume show a further decrease for the TiO_2 aerogels heat-treated at 400 °C and 500 °C, indicating a decrease in porosity. This is in accordance with the results reported in literature for calcined aerogel samples.[6] Even though the calcination of the TiO_2 aerogel reduced the specific surface area and porosity, both are higher compared to conventional bulk anatase, and therefore it is beneficial using the investigated sol-gel synthesis conditions and supercritical drying for TiO_2 aerogel synthesis.[6]

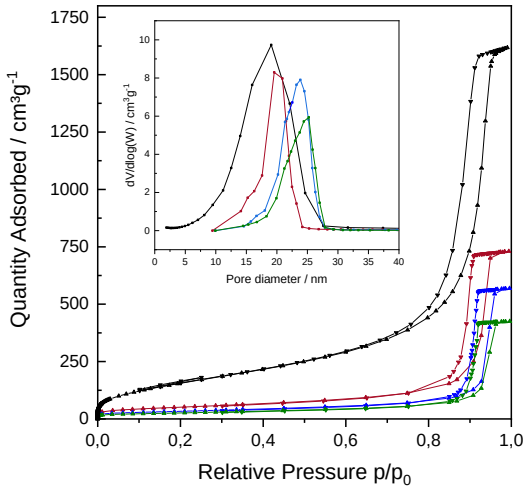

Figure 2. N_2 physisorption isotherms and BHJ pore size distribution (inset) for the as-synthesized and heat-treated TiO_2 aerogels; as-synthesized TiO_2 aerogel (black) and aerogels calcined at 300 °C (red), 400 °C (blue) and 500 °C (green).

Table 2. Nitrogen physisorption results and band gaps of the prepared TiO_2 aerogel samples.

	BET surface area / $m^2\ g^{-1}$	Cumulative pore volume / $cm^3\ g^{-1}$	Average pore diameter / nm	Band gap/ eV
as-synthesized	600	2.5	19	3.5
300 °C	184	1.1	20	3.3
400 °C	118	0.9	24	3.3
500 °C	92	0.7	25	3.2

Figure 3 shows the SEM images of the different TiO_2 aerogels at two different magnifications. The as-synthesized sample (a) shows mainly a smooth surface. The high magnification SEM image (b) shows small, nearly spherical interconnected particles which form an open porous network. This is highlighted with dotted lines in **Figure 3b**. **Figure 3** c-h show the SEM images of the heat-treated TiO_2 aerogels at 300 °C, 400 °C and 500 °C. The images show also a smooth uniform surface of the samples, however the porosity of the samples decreases with higher calcination temperature, which is visible through the fewer and larger voids/pores between the particles and denser appearance of the microstructure. The particles become larger with higher calcination temperature and seem to be arranged more densely.

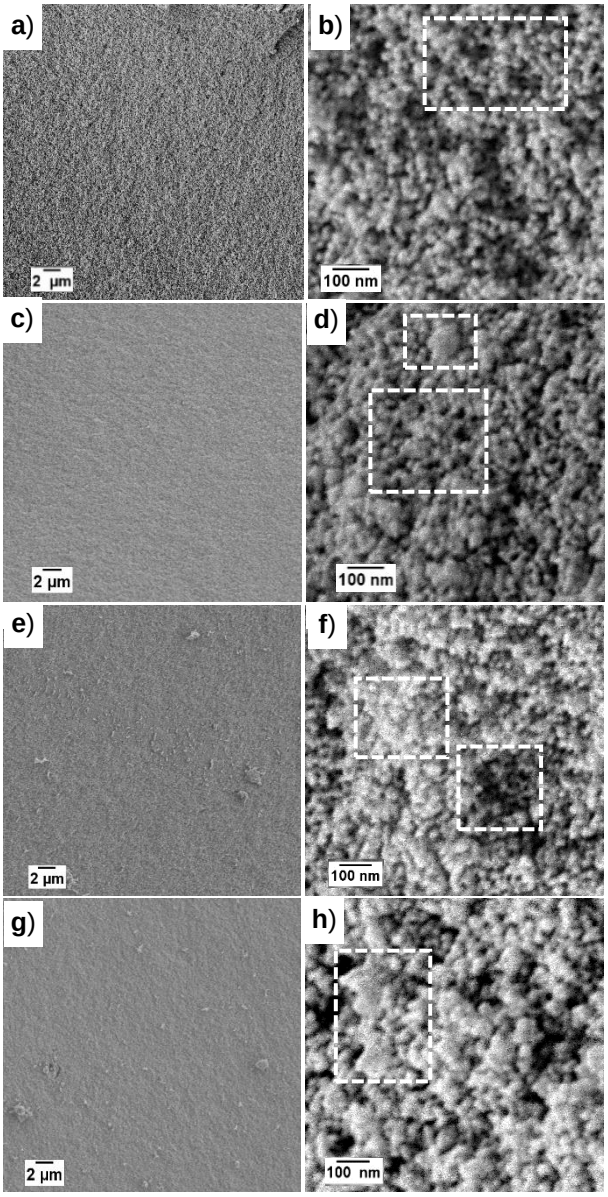

Figure 3. SEM images of the a-b) as-synthesized aerogel, c-d) calcined aerogel at 300 °C, e-f) calcined aerogel at 400 °C, g-h) calcined aerogel at 500 °C, at lower (5.000x) and higher (100.000x) magnification.

In **Figure 3d** small pores are still visible but also larger particles at 300°C calcination temperature compared to the as-synthesized sample. The effect of higher calcination temperature leading to larger pores and denser microstructure gets clearly visible at 400°C calcination temperature in the highlighted areas in **Figure 3f**. The particle size increases at 500°C calcination temperature, which is highlighted in **Figure 3h**. These results are in good agreement with the N_2 physisorption results in **Figure 2** and **Table 2**.The as-synthesized TiO_2 aerogel was further analyzed using TEM, to confirm the observed semi-crystalline structure. **Figure 4** shows the TEM images of the as-synthesized TiO_2 aerogel at different magnifications. Amorphous particles and nanocrystals can be observed. This is in good agreement with the XRD results shown in **Figure 1**, where a semi-crystalline structure was assumed. The TEM image shows the interconnected particles and nanocrystals in the porous network. It can be assumed that the particles in the aerogel network are connected by chemical means, rather than physical connection as in P25 nanopowder. This is advantageous for photocatalytic hydrogen evolution, as this could improve the separation of charge carriers. It was reported that the interconnected structure of TiO_2 nanocrystals offers better charge carrier delocalization compared to TiO_2 nanoparticle aggregates, e.g. P25 which are physically connected.[17,42] The inset in **Figure 4** shows the d-spacing which was estimated 0.35 nm for the observed nanocrystals. This fits to the (101)-oriented anatase TiO_2 phase and confirms the semi-crystalline nature of the as-synthesized TiO_2 aerogel.

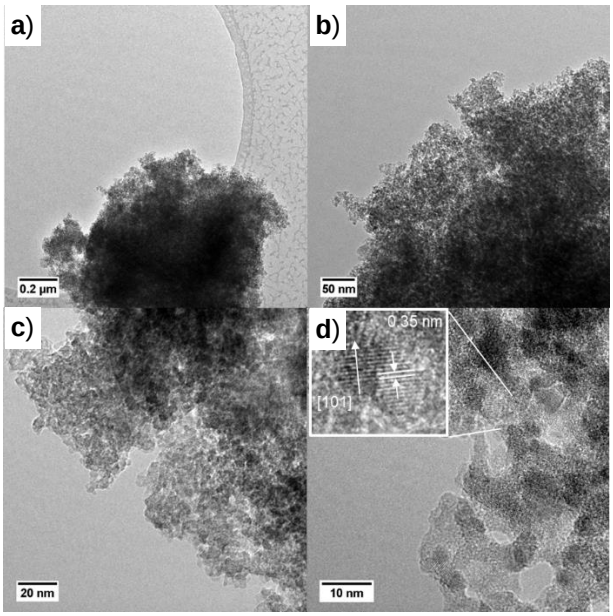

Figure 4. TEM images of as-synthesized TiO_2 aerogel, a) 12.000x, b) 39.000x, c) 115.000x, d) 295.000x, the inset is a local enlargement of TiO_2 nanocrystal.

The size of the nanocrystals was estimated approx. 4-6 nm, which is slightly larger compared to the calculated grain size from XRD pattern (approx. 4 nm). This partial crystallinity is confirmed via basic Rietveld refinement. The amount of amorphous phase is decreased via heat treatment from initial 10wt.% for the as-synthesized aerogel to none (within the boundaries of the error).

Absorption spectra in diffuse reflectance were recorded to characterize the optical properties of the TiO_2 aerogels. Diffuse reflectance spectra was converted to Kubelka-Munk spectra and Tauc plots for band gap estimation (**Figure S1**). **Table 2** shows the estimated band gaps of the aerogel samples. The bandgap of the untreated TiO_2 aerogel is with 3.5 eV slightly higher than the bandgap of the calcined aerogels with 3.2 to 3.3 eV, which was expected as it is a partially amorphous sample. For all aerogels, only one sharp absorption edge at 340 to 375 nm is visible in the UV-vis spectra, indicating that no by-phases are formed. The estimated bandgaps are in correspondence with the reported literature values for anatase TiO_2 with 3.2 eV.[42,43]

3.2 Photocatalytic electron storage and hydrogen generation

Photocatalytic experiments were performed with all TiO_2 aerogel samples to investigate the influence of the physicochemical properties of the aerogels on the electron storage capability and photocatalytic activity (**Figure 5**). For this, 100 mg aerogel were dispersed in 150 mL of a 2.5 mol L^{-1} aqueous methanol solution, and were irradiated with a 300 W Xe lamp (see *Experimental Section*). The samples were first irradiated for 100 minutes without a co-catalyst. The color change of the dispersions is shown in the graph (**Figure 5**) going from a colorless dispersion to a blueish colored dispersion after irradiation. Enlarged versions of the photographs are given additionally in the *Supporting information* (**Figure S2** SI). This blue coloration is an indication of the storage of electrons and formation of Ti^{3+} states.[22,24,26,44] Their recombination is inhibited due to the use of methanol as hole scavenger, reacting fast with photogenerated holes.[21]

The intensity of the blue color decreases with increasing calcination temperature of the aerogels, and therefore also with the surface area of the TiO_2 aerogel samples. Meanwhile, the amounts of detected hydrogen are very low (below 10 µmol h^{-1}), as expected for unmodified TiO_2. Indeed, the sample with the smallest surface area - calcined at 500 °C - offers the best hydrogen evolution rate up to 3.2 µmol h^{-1}. It can be assumed that the interconnection of the TiO_2 nanocrystals in the aerogels improves by higher calcination temperature, which is

advantageous for the photocatalytic hydrogen production, as the charge carrier separation seems to be improved. The heat-treatment can also reduce the amount of bulk defects, which are recombination centers. Kong *et al.* reported a reduced bulk to surface defect ratio and increased photocatalytic activity for TiO_2 nanocrystals, which were calcined compared to TiO_2 nanocrystals, which were prepared without a calcination step.[45]

After the lamp was switched off and the hydrogen evolution went to zero, an aqueous H_2PtCl_6 solution was added to the blueish dispersions *via* rubber sealing (to keep the inert atmosphere in the reactor), to achieve Pt decoration *via* subsequent photodeposition. However, even before continuing the light irradiation but few seconds after the addition of the co-catalyst precursor solution, the coloration of the dispersion disappeared. At the same time, a sharp peak in the hydrogen evolution rate was detected in all four cases. The intensity of this hydrogen evolution peak without light irradiation has the same trend as the intensity of the blueish color of the dispersion: The darker the dispersion before H_2PtCl_6 addition, the higher the hydrogen evolution peak after the addition, up to 20 µmol h^{-1}.

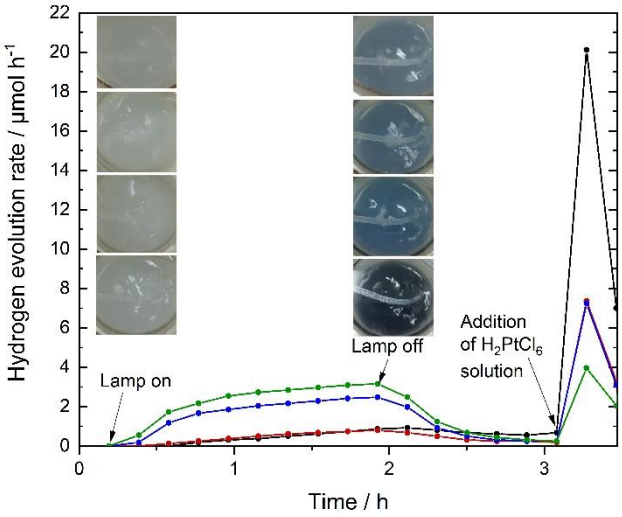

Figure 5. Hydrogen evolution rates over time of the as-synthesized (black) and calcined TiO_2 aerogels, 300 °C (red), 400 °C (blue), 500 °C (green); Measured without co-catalyst for the first 100 min; measured with 0.0076 µmol m^{-2} Pt as co-catalyst (≙ 0.1 wt.-% for the as-synthesized sample) for approx. 30 min without irradiation. The photographs show the dispersions before irradiation, and after 100 min irradiation with 500 °C, 400 °C, 300 °C and as-synthesized sample from top to bottom.

This hydrogen evolution rate peak can be explained by the photogenerated and stored electrons in the aerogel sample being used to form metallic Pt clusters on the TiO_2 aerogels upon H_2PtCl_6 reduction. After all Pt ions are reduced and formed Pt metal nanoparticles, a Schottky contact is formed between Pt and TiO_2, upon which the excess stored electrons in the aerogels are transferred to the Pt metal particles, were they are used to reduce protons to hydrogen acting as co-catalysts. This is then detected as the sharp peak in the hydrogen evolution rate curve. This kind of mechanism was already reported before for different metal co-catalyst deposition on TiO_2.[22,23,44,46] The intensity of this peak is therefore - beneath the intensity of the blue color – an indication for the amount of stored electrons. Furube *et al.* reported an improved charge carrier separation by Pt deposition on TiO_2 by use of transient absorption spectroscopy, which additionally explains the enhancement of the hydrogen evolution rate.[47]

The electron storage capability of the aerogels can be related to their physicochemical properties. The as-synthesized partially amorphous sample with the highest surface area can store the most electrons indicated by the most intense blue coloration. Ikeda *et al.* reported that electrons are trapped at defective sites in TiO_2 e.g. oxygen vacancies, which are mainly located at the surface of TiO_2. They state that the quantity of accumulated electrons represents the number of defective sites.[48] The as-synthesized aerogel can therefore store the most photocharged electrons due to the highest surface area and presumably highest amount of surface defects, due to its low heat treatment. An increase in the heat treatment and decrease in surface area results in a decreased amount of stored electrons.

In case of the semi-crystalline as-synthesized TiO_2 aerogel, more electrons are stored in the material and are not used for the hydrogen evolution, as can be seen in the coloration of the dispersion. This is an indication that the electrons are trapped in surface defects and not in bulk defects, where electrons would recombine with holes. Surface defects are on the one hand charge carrier traps and on the other hand adsorption sites for methanol as hole scavenger.[45] Electrons are trapped, recombination is prevented by the fast and efficient reaction of the holes with methanol, which makes the untreated aerogel the best electron storage material in this study. Heat treatment seems to reduce the amount of surface defects and bulk defects leading to reduced electron storage, but improved charge carrier separation and hydrogen evolution.

The dependence on the heat treatment of the aerogel can be seen also in the photocatalytic hydrogen evolution rates after co-catalyst deposition (**Table 3**). After the deposition of the co-catalyst, no blue coloration of the dispersion can be observed anymore (**Figure S2**), as the electrons are transferred to the formed metallic Pt particles where they are used for the hydrogen evolution

and not stored in the material. All samples exhibit the same amount of co-catalyst, nevertheless a clear difference in the activity is observed. As the Pt particles prevent the storage of the electrons in surface defect states, the difference in the activity can be explained by the heat treatment and the amount of bulk defects. The heat-treated aerogels show a decreased charge carrier recombination and therefore higher activity compared to the semi-crystalline aerogel. This can be explained by the decreased number of surface and bulk defects due to the calcination process as well as the photocatalytic activity of exposed facets of the crystalline phase.[49] The photocatalytic activity is also improved by the sintered and chemically linked TiO_2 nanoparticles, due to the wide distribution and therefore better separation of charge carriers, up to 340 µmol h^{-1} for the aerogel calcined at 500 °C (**Table 3**).[17]

Table 3. Hydrogen evolution rates of the prepared TiO_2 aerogel samples.

	Hydrogen evolution rate (with 0.1 wt.-% Pt) / µmol h^{-1}
as-synthesized	25.5
300 °C	176.5
400 °C	279.2
500 °C	331.8

The TiO_2 aerogels were all regained after the photocatalytic hydrogen experiments by washing and supercritical drying. XRD pattern after the photocatalytic hydrogen production experiments are shown in **Figure S3**. The XRD pattern of the heat treated aerogels show no changes, the small amounts of Pt added are not visible. Interestingly, the as-synthesiszed aerogel sample exhibits more pronounced reflections than before the experiments, but offers still a semi-crystalline character. Rietveld refinement indicated an increase of crystallinity of the as-synthesized TiO_2 aerogel after UV irradiation/photocatalytic hydrogen experiment from approx. 10 wt.% to 40 wt.% crystalline content. Zywitzki *et al.* already showed that amorphous TiO_2 can be prepared by an UV-light mediated synthesis using $Ti(OEt)_4$ as titanium alkoxide precursor. The increase of crystallinity of the as-synthesized aerogel after UV-light exposure could be related to the UV irradiation with the Xe lamp used in the experiment. This will be further investigated in future studies.[44]

We showed that the material properties of the aerogels have a direct influence on the electron storage capability. To verify the differences in the amount of stored electrons in the aerogel samples, the absorbance of the aerogel dispersions was measured in the range between 350 nm to 800 nm before and after irradiation of the experiment shown in Figure 5. To detect the time-dependent fading in the absorbance, the absorbance was determined directly after the irradiation for 100 min, 30 min after irradiation stop, and 110 min after irradiation (**Figure S4**). For this test, dispersions of 100 mg of the TiO_2 aerogel in 150 mL of a 2.5 mol L^{-1} aqueous methanol solution were irradiated. The increase in absorption of the dispersions after the irradiation for 100 min (charging) was detected at a wavelength of 600 nm and compared to the absorbance of the dispersion before irradiation (**Figure 6**). The absorbance increase directly after irradiation for 100 min is most prominent in the as-synthesized aerogel and the aerogel calcined at 300 °C, being lower for higher calcination temperatures of the aerogel. This is in good agreement to the photographs taken and shown in Figure 5. A decay in absorbance increase after irradiation is most prominent for the sample calcined at 300 °C, and also detectable in the as-synthesized aerogel. For higher calcined samples, hardly any decay of the absorption increase is detectable in the investigated time range. The decay in the absorbance is attributable with a decreasing amount of stored electrons in the aerogel sample, which can be due to charge carrier recombination or either reduction reaction. Electron storage is preferred in aerogel samples with lower heat treatment, which goes directly in line with reduced rates for photocatalytic hydrogen evolution, in accordance with the photocatalysis results.

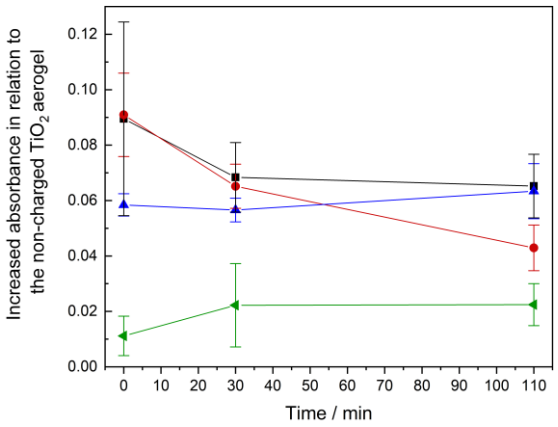

Figure 6. Absorption changes measured after charging of as-synthesized (black) and calcined TiO_2 aerogels, 300 °C (red), 400 °C (blue), 500 °C (green) (top). The increase in absorbance at 600 nm after 100 min irradiation (charging, = 0 min) is given, followed by two additional measurements (30 min or 110 min after irradiation, respectively) without irradiation indicating color fading (bottom).

Since the results lead to the conclusion that the as-synthesized aerogel seems to offer the best electron storage ability, further experiments were performed with this sample.

Commercial anatase nanoparticles were measured in comparison to the as-synthesized TiO_2 aerogel to show the benefit of the aerogel prepared in the present work

(**Figure S5**). The as-synthesized aerogel shows a better electron storage ability shown by the intense coloration compared to commercial anatase nanoparticles.
The influence of electron storage ability on the methanol concentration was additionally tested. Dispersions of 100 mg of the aerogel in 150 mL aqueous solution with different methanol concentrations ranging from 0.02 mol L^{-1} up to 19.7 mol L^{-1} were irradiated for 100 min while simultaneously hydrogen evolution was detected. Additionally, photographs of the dispersions were taken directly after the irradiation (**Figure 7**), enlarge versions of the photograph are given in the *Supporting Information* (**Figure S6**). All dispersions show the typical blue coloration as indication of the storage of electrons and formation of Ti^{3+} states. Only a very slight coloration and presumably small amount of stored electrons are visible for the lowest methanol concentration of 0.02 mol L^{-1} after irradiation for 100 min. This goes in line with a negligible amount of evolved hydrogen. For all other methanol concentrations higher than 0.02 mol L^{-1}, a comparable hydrogen evolution rate between 0.8 and 1.1 µmol h^{-1} is detected. The higher the methanol concentration, the darker is the coloration of the dispersion after the same time of irradiation. Thus, the amount of stored electrons can be adjusted by the used methanol concentration. The higher the concentration of the hole scavenger is, the higher the amount of stored electrons, with hardly any changes in hydrogen evolution rates. From these results, it can be assumed that in case of very small amount of hole scavenger, the recombination rate at the surface defects is increased as the holes cannot react with methanol before recombining with trapped electrons. The higher the concentration of the hole scavenger, the more methanol can adsorb on surface defects and the charge carrier recombination is strongly reduced, which is visible in an increased coloration of the dispersion – an increased number of stored electrons and therefore Ti^{3+} states in the sample. This further supports the results from the hydrogen evolution experiments. These results pave the way for future hydrogen-on-demand application, when charging and hydrogen evolution can be spatially and timely separated.

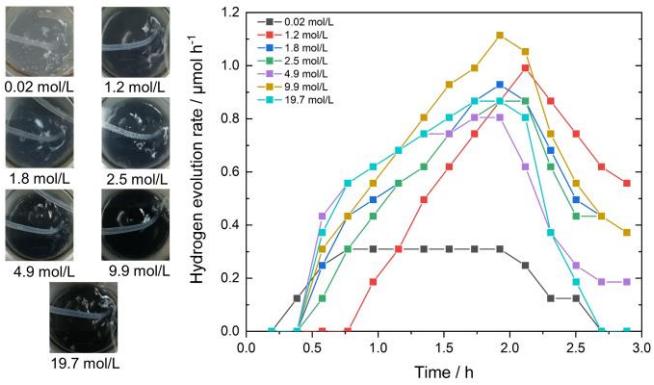

Figure 7. Hydrogen evolution rates over time of the as-synthesized TiO_2 aerogel dispersed in aqueous methanol solutions with different methanol concentrations, plus photographs of the dispersions after an irradiation time of 100 min. Irradiation was stopped after 100 min.

A material like the here presented as-synthesized TiO_2 aerogel with high electron storage ability and high amount of surface defects offers the possibility to apply it for other reactions, for example in dark reduction reactions of very stable molecules. One of the currently most investigated reactions of this type is for example the nitrogen reduction reaction.[50,51] Surface oxygen vacancies can be beneficial for the N_2 adsorption and conversion, which makes the as-synthesized TiO_2 aerogel an interesting material for this research area.[52] Furthermore, Bahnemann *et al.* showed in 2011, that photoexcited electrons stored in TiO_2 colloids can reduce N_2.[21] Therefore, a similar experiment with the as-synthesized TiO_2 aerogel was performed. 100 mg of the as-synthesized aerogel sample was dispersed in 150 mL of an aqueous 2.5 mol L^{-1} methanol solution and irradiated for 100 min under argon to store electrons in the sample. Subsequently, the lamp was turned off and the gas was switched to nitrogen, flushing through the dispersion for 7 hours. Afterwards, a salicylate test was performed to determine the amount of produced ammonia. **Figure S7** shows the absorbance spectra of this salicylate test. An absorbance peak is visible after the reaction time of 7 hours, which related to an obtained ammonia yield of 5 µg L^{-1}. This positive test for dark nitrogen reduction reaction with stored photogenerated electrons on an as-synthesized TiO_2 aerogel sample gives rise to future research work on such aerogels for photocatalytic ammonia generation.

4. Conclusion

Mesoporous TiO_2 aerogels with large surface areas were prepared *via* acid-catalyzed sol-gel synthesis and supercritical drying. As-synthesized and calcined TiO_2 aerogels at 300, 400 and 500 °C exhibit surface area of 600, 184, 118 and 92 m^2 g^{-1}, respectively. Interestingly,

even without calcination, the as-synthesized aerogel is partly crystalline with anatase crystallites.

TiO_2 aerogels are able to store photogenerated electrons in surface trap states upon illumination in water-methanol dispersions. The capacity to store photogenerated electrons increases with lower calcination temperature. Furthermore, the extent of electron storage also depends on the methanol scavenger concentration. We plan to quantify the electron storage capacity with transient absorption spectroscopy in the future.

Increasing the calcination temperature to 500 °C results in decreased surface area, however in strongly increased hydrogen evolution rates in photocatalytic experiments. Finally, nitrogen reduction to ammonia in the dark was performed with photogenerated stored electrons in TiO_2 aerogels, separating the charge carrier photogeneration from the nitrogen reduction reaction. This result paves the way for future application of such tailored and cheap TiO_2 aerogels in solar fuel-on-demand processes.

Acknowledgements

We thank Judith Zander (University of Bayreuth) for support in the NRR experiment, Markus Heyer (DLR) for support in supercritical drying, Dr. Peter Mechnich (DLR) and Alexander Francke (DLR) for support in X-ray quantitative phase analysis.

Conflict of interest

The authors declare no conflict of interest.

References

1 N. Hüsing and U. Schubert, *Angew. Chemie - Int. Ed.*, 1998, 37, 22–45.

2 S. Alwin and X. Sahaya Shajan, *Mater. Renew. Sustain. Energy*, 2020, 9, 3.

3 K. C. Song and S. E. Pratsinis, *J. Am. Ceram. Soc.*, 2001, **84**, 92–98.

4 H. Choi, M. Carboni, Y. K. Kim, C. H. Jung, S. Y. Moon, M. M. Koebel and J. Y. Park, *Catal. Letters*, 2018, **148**, 1504–1513.

5 H. Schäfer, B. Milow and L. Ratke, *RSC Adv.*, 2013, **3**, 15263–15272.

6 S. Sadrieyeh and R. Malekfar, *J. Non. Cryst. Solids*, 2017, **457**, 175–179.

7 M. L. Anderson, R. M. Stroud, C. A. Morris, C. I. Merzbacher and D. R. Rolison, *Adv. Eng. Mater.*, 2000, 2, 481–488.

8 A. L. Luna, F. Matter, M. Schreck, J. Wohlwend, E. Tervoort, C. Colbeau-Justin and M. Niederberger, *Appl. Catal. B Environ.*, 2020, **267**, 118660.

9 V. G. Parale, T. Kim, V. D. Phadtare, H. M. Yadav and H. H. Park, *J. Mol. Liq.*, 2019, **277**, 424–433.

10 T. Kim, V. Parale, H.-N.-R. Jung, Y. Kim, Z. Driss, D. Driss, A. Bouabidi, S. Euchy and H.-H. Park, *Nanomaterials*, 2019, **9**, 358.

11 V. G. Parale, T. Kim, K. Y. Lee, V. D. Phadtare, R. P. Dhavale, H. N. R. Jung and H. H. Park, *Ceram. Int.*, 2020, **46**, 4939–4946.

12 J. C. Bernardes, G. K. Pinheiro, D. Muller, E. Latocheski, J. B. Domingos and C. R. Rambo, *J. Sol-Gel Sci. Technol.*, 2020, **94**, 425–434.

13 P. A. DeSario, J. J. Pietron, D. H. Taffa, R. Compton, S. Schünemann, R. Marschall, T. H. Brintlinger, R. M. Stroud, M. Wark, J. C. Owrutsky and D. R. Rolison, *J. Phys. Chem. C*, 2015, **119**, 17529–17538.

14 D. A. Panayotov, P. A. Desario, J. J. Pietron, T. H. Brintlinger, L. C. Szymczak, D. R. Rolison and J. R. Morris, *J. Phys. Chem. C*, 2013, **117**, 15035–15049.

15 S. K. Parayil, R. J. Psota and R. T. Koodali, *Int. J. Hydrogen Energy*, 2013, **38**, 10215–10225.

16 J. Kwon, K. Choi, M. Schreck, T. Liu, E. Tervoort and M. Niederberger, *ACS Appl. Mater. Interfaces*, 2021, **13**, 53691–53701.

17 C. C. Lin, T. Y. Wei, K. T. Lee and S. Y. Lu, *J. Mater. Chem.*, 2011, **21**, 12668–12674.

18 J. Puskelova, L. Baia, A. Vulpoi, M. Baia, M. Antoniadou, V. Dracopoulos, E. Stathatos, K. Gabor, Z. Pap, V. Danciu and P. Lianos, *Chem. Eng. J.*, 2014, **242**, 96–101.

19 Y. Di Iorio, M. E. Aguirre, M. A. Brusa and M. A. Grela, *J. Phys. Chem. C*, 2012, **116**, 9646–9652.

20 M. Sachs, E. Pastor, A. Kafizas and J. R. Durrant, *J. Phys. Chem. Lett.*, 2016, **7**, 3742–3746.

21 D. Bahnemann, A. Henglein, J. Lilie and L. Spanhel, *J. Phys. Chem.*, 1984, **88**, 709–711.

22 H. H. Mohamed, R. Dillert and D. W. Bahnemann, *J. Phys. Chem. C*, 2011, **115**, 12163–12172.

23 H. H. Mohamed, R. Dillert and D. W. Bahnemann, *Chem. - A Eur. J.*, 2012, **18**, 4314–4321.

24 H. H. Mohamed, R. Dillert and D. W. Bahnemann, *J. Photochem. Photobiol. A Chem.*, 2011, **217**, 271–274.

25 H. H. Mohamed, R. Dillert and D. W. Bahnemann, *J. Photochem. Photobiol. A Chem.*, 2012, **245**, 9–17.

26 H. H. Mohamed, C. B. Mendive, R. Dillert and D. W. Bahnemann, *J. Phys. Chem. A*, 2011, **115**, 2139–2147.

27 M. Sakar, C. C. Nguyen, M. H. Vu and T. O. Do, *ChemSusChem*, 2018, **11**, 809–820.

28 C. Ng, A. Iwase, Y. H. Ng and R. Amal, *ChemSusChem*, 2013, **6**, 291–298.

29 M. Schulz, N. Hagmeyer, F. Wehmeyer, G. Lowe, M. Rosenkranz, B. Seidler, A. Popov, C. Streb, J. G. Vos and B. Dietzek, *J. Am. Chem. Soc.*, 2020, **142**, 15722–15728.

30 V. W. Lau and B. V. Lotsch, *Adv. Energy Mater.*, 2021, 2101078.

31 J. Kröger, A. Jiménez-Solano, G. Savasci, P. Rovó, I. Moudrakovski, K. Küster, H. Schlomberg, H. A. Vignolo-González, V. Duppel, L. Grunenberg, C. B. Dayan, M. Sitti, F. Podjaski, C. Ochsenfeld and B. V. Lotsch, *Adv. Energy Mater.*, , DOI:10.1002/aenm.202003016.

32 L. Zhou and C. E. Boyd, *Aquaculture*, 2016, **450**, 187–193.

33 J. C. Bernardes, D. Müller, G. K. Pinheiro and C. R. Rambo, *Opt. Mater. (Amst).*, 2020, **109**, 110359.

34 S. Alwin, V. Ramasubbu and X. Sahaya Shajan, *Bull. Mater. Sci.*, 2018, **41**, 27.

35 Y. Quintero, E. Mosquera, J. Diosa and A. García, *J. Sol-Gel Sci. Technol.*, 2020, **94**, 477–485.
36 S. A. Lermontov, E. A. Straumal, A. A. Mazilkin, A. E. Baranchikov, B. B. Straumal and V. K. Ivanov, *Mater. Lett.*, 2018, **215**, 19–22.
37 R. Moussaoui, K. Elghniji, M. ben Mosbah, E. Elaloui and Y. Moussaoui, *J. Saudi Chem. Soc.*, 2017, **21**, 751–760.
38 T. A. Kandiel, R. Dillert, L. Robben and D. W. Bahnemann, *Catal. Today*, 2011, **161**, 196–201.
39 M. Thommes, K. Kaneko, A. V Neimark, J. P. Olivier, F. Rodriguez-Reinoso, J. Rouquerol and K. S. W. Sing, , DOI:10.1515/pac-2014-1117.
40 C. Schlumberger and M. Thommes, *Adv. Mater. Interfaces*, 2021, **8**, 2002181.
41 R. Bardestani, G. S. Patience and S. Kaliaguine, *Can. J. Chem. Eng.*, 2019, 97, 2781–2791.
42 P. Voepel, M. Weiss, B. M. Smarsly and R. Marschall, *J. Photochem. Photobiol. A Chem.*, 2018, **366**, 34–40.
43 C. Dette, M. A. Pérez-Osorio, C. S. Kley, P. Punke, C. E. Patrick, P. Jacobson, F. Giustino, S. J. Jung and K. Kern, *Nano Lett.*, 2014, **14**, 6533–6538.
44 D. Zywitzki, H. Jing, H. Tüysüz and C. K. Chan, *J. Mater. Chem. A*, 2017, **5**, 10957–10967.
45 M. Kong, Y. Li, X. Chen, T. Tian, P. Fang, F. Zheng and X. Zhao, *J. Am. Chem. Soc.*, 2011, **133**, 16414–16417.
46 J. Kiwi and M. Grätzel, *J. Phys. Chem.*, 1984, **88**, 1302–1307.
47 A. Furube, T. Asahi, H. Masuhara, H. Yamashita and M. Anpo, *Chem. Phys. Lett.*, 2001, **336**, 424–430.
48 S. Ikeda, N. Sugiyama, S. Murakami, H. Kominami, Y. Kera, H. Noguchi, K. Uosaki, T. Torimoto and B. Ohtani, *Phys. Chem. Chem. Phys.*, 2003, **5**, 778–783.
49 J. Yan, G. Wu, N. Guan, L. Li, Z. Li and X. Cao, *Phys. Chem. Chem. Phys.*, 2013, **15**, 10978.
50 D. Ziegenbalg, J. Zander and R. Marschall, *ChemPhotoChem*, 2021, **5**, 792–807.
51 M. Cheng, C. Xiao and Y. Xie, *J. Mater. Chem. A*, 2019, 7, 19616–19633.
52 C. Li, T. Wang, Z.-J. Zhao, W. Yang, J.-F. Li, A. Li, Z. Yang, G. A. Ozin and J. Gong, *Angew. Chemie*, 2018, **130**, 5376–5380.

Supporting Information

Photocatalytic activity and electron storage ability of TiO_2 aerogels with adjustable surface area

Alexandra Rose[a]§, *Anja Hofmann*[b]§, *Pascal Voepel*[a], *Barbara Milow*[a], *Roland Marschall*[b]

[a] A. Rose, Dr. P. Voepel, Prof. B. Milow
German Aerospace Center
Institute of Materials Research
Aerogels and Aerogel composites
Linder Höhe, Köln 51147, Germany

[b] A. Hofmann, Prof. R. Marschall
Department of Chemistry
University of Bayreuth
Universitätsstraße 30, Bayreuth 95447, Germany
E-mail: roland.marschall@uni-bayreuth.de , ORCID: 0000-0002-1057-0459

§: These authors contributed equally to the manuscript.

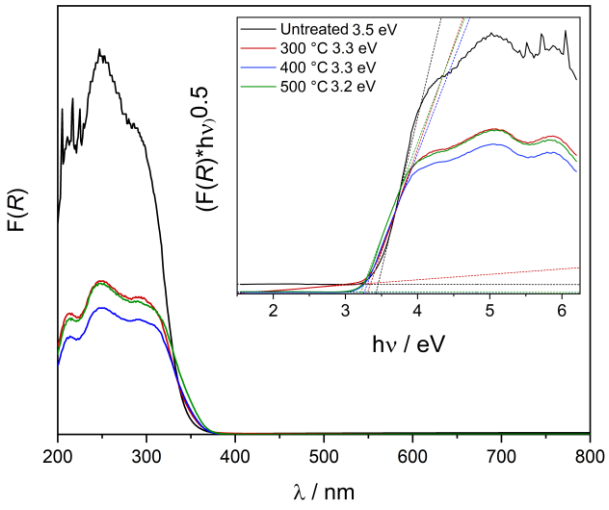

Figure S1. Kubelka-Munk UV-vis spectra and Tauc plots (inset) of the as-synthesized aerogel (black), the 300 °C (red), the 400 °C (blue), and the 500 °C (green) calcined aerogels.

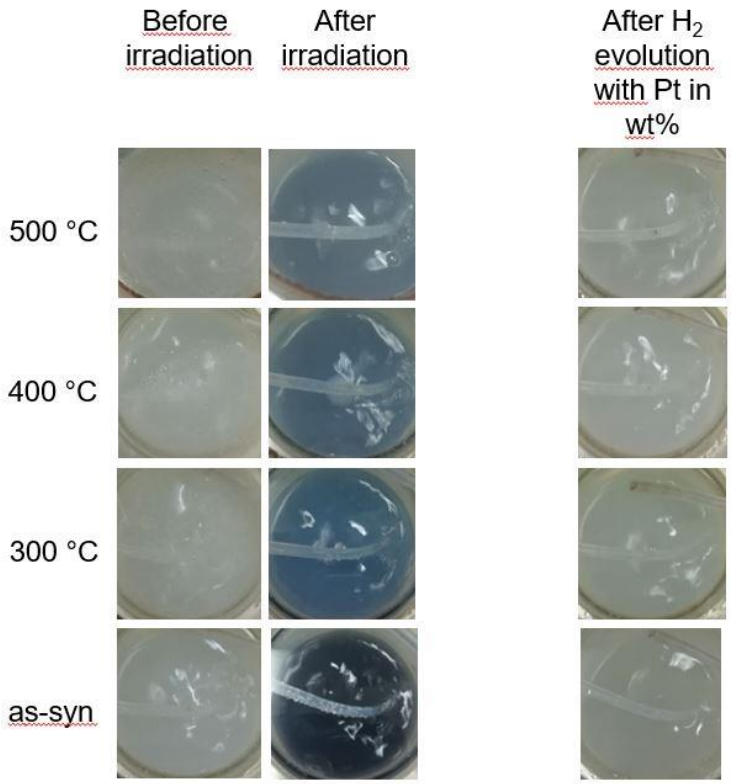

Figure S2: Enlarged photographs from Figure 5, showing the coloration of the different photocharged aerogel dispersions.

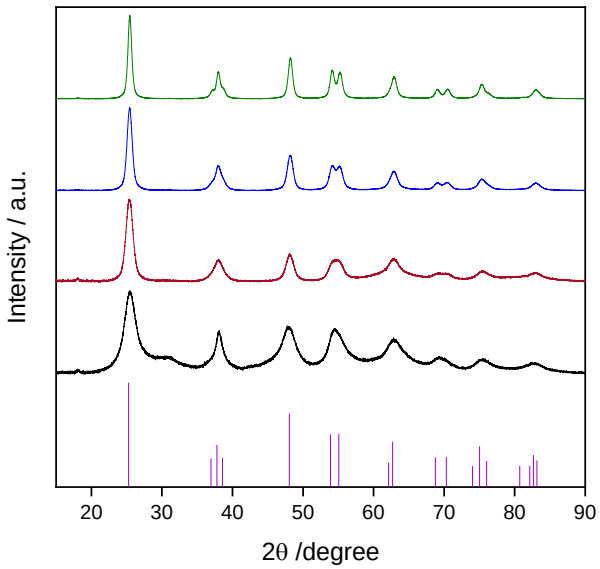

Figure S3. XRD patterns of the as-synthesized TiO_2 aerogel (black) and aerogels calcined at 300 °C (red), 400 °C (blue) and 500 °C (green) after photocatalytic hydrogen production reaction. Reference pattern of anatase TiO_2 (PDF-21-1272) is shown for comparison. Normalized data to the range 0 to 100 related to the highest signal.

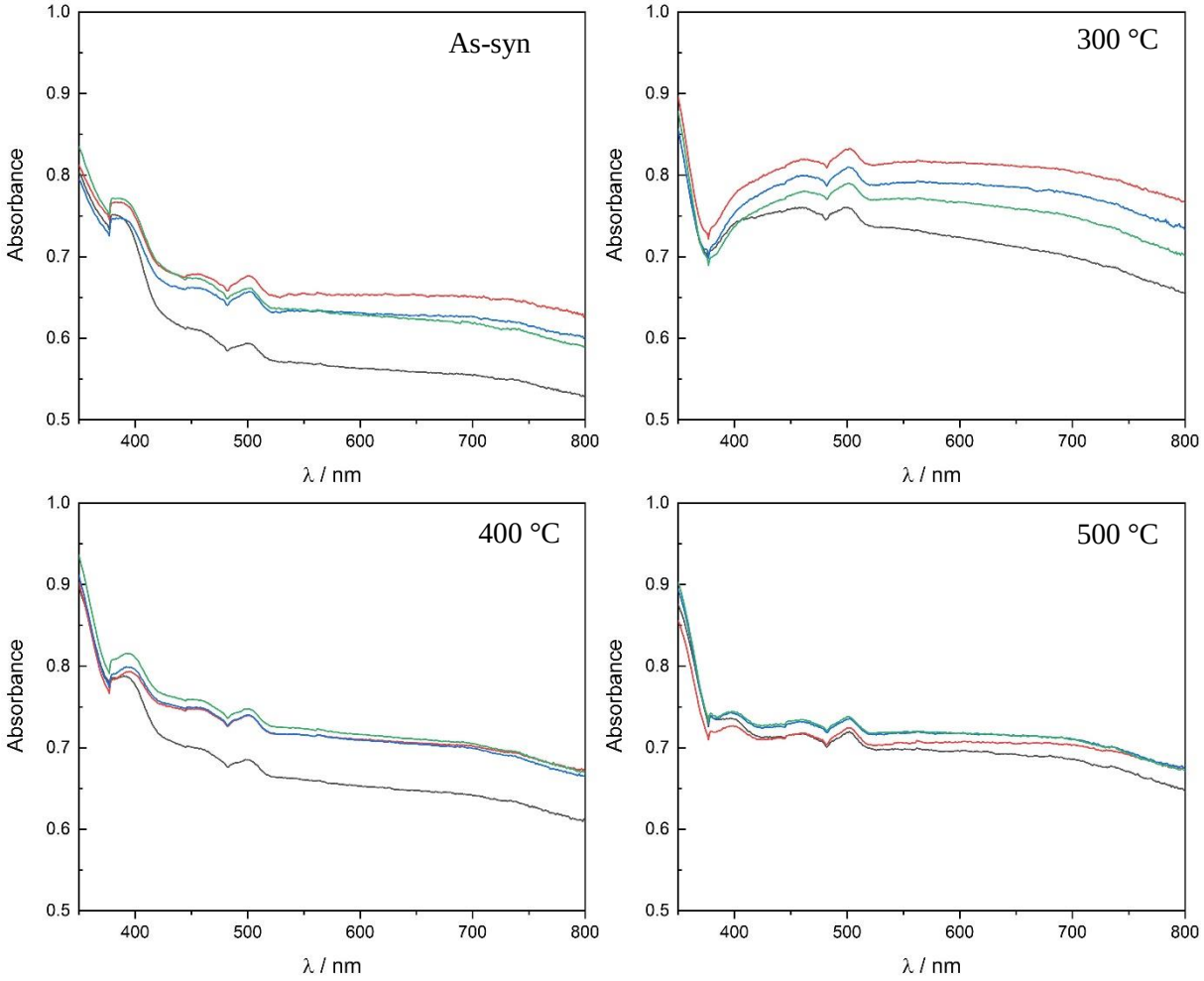

Figure S4. Absorbance measurements of the four TiO_2 aerogels dispersions, before irradiation (gray), directly after 100 min of irradiation (green), 30 min after irradiation (blue) and 1 h 50 min after irradiation (red).

Figure S5: Comparison of the electron storage ability of as-syn TiO2 aerogel and commercial anatase nanoparticles. Lamp was turned on after 30 minutes and off after 90 minutes irradiation. For this comparison

50 mg of the corresponding sample was used for the measurement, a 300 W Xe lamp and a 10% methanol solution.

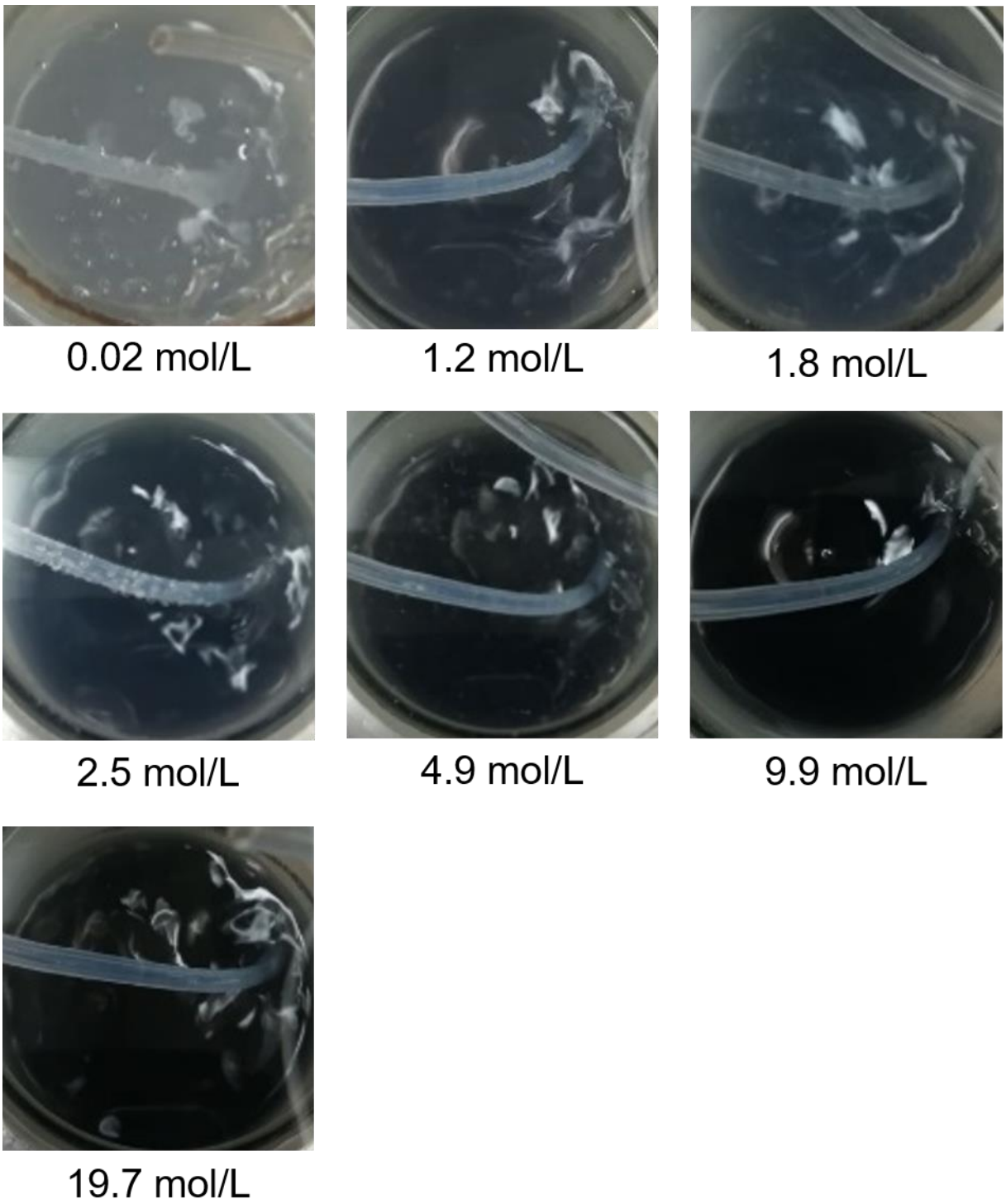

Figure S6: Enlarged photographs of photocharged TiO_2 aerogel dispersion with different MeOH concentration in water.

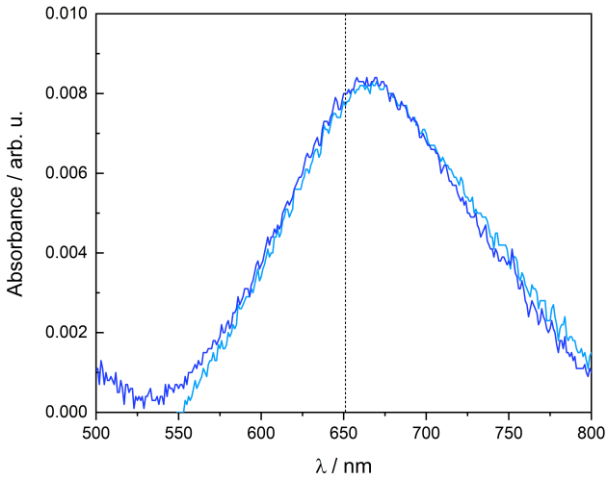

Figure S6. Absorbance spectra of the salicylate test of the solution of nitrogen reduction reaction with and as-synthesized TiO_2 aerogel sample for determination of the obtained NH_3 concentration. The test was performed two times to verify the result. The dashed line is the absorbance maximum, which was used for the calibration.